

Parametric scattering of microcavity polaritons into ghost branches

Joanna M Zajac* and Wolfgang Langbein
 School of Physics and Astronomy, Cardiff University,
 The Parade, Cardiff CF24 3AA, United Kingdom
 (Dated: November 21, 2018)

Polaritons of defined momentum and energy are excited resonantly on the lower polariton branch of a planar semiconductor microcavity in the strong coupling regime, and the spectrally and momentum resolved emission is analyzed. We observe ghost branches from scattering within the lower polariton branch, as well as from scattering to the middle polariton branch, showing the non-linear mixing between different branches. Extending the theoretical treatment of spontaneous parametric luminescence developed in Ciuti *et al.*, Phys. Rev. B **63**, 041303 (2001), the eigenmodes of the driven polariton system and its photoluminescence are modeled.

Cavity excitons-polaritons in planar semiconductor microcavities are quasi-particles resulting from strong coupling between the Fabry-Pérot cavity mode and excitonic resonance of the semiconductor inside the cavity. Below the exciton saturation density, polaritons can be treated as composite bosons¹. They inherit features of exciton and photon constituents resulting in strong interactions and a in-plane dispersion and propagation dominated by the cavity mode. The parametric scattering of microcavity polaritons is described in lowest order by the third-order susceptibility². Given a coherent population of "pump" (P) polaritons, which are scattered into "signal" (S) and "idler" (I) polaritons, the phase matching in time and space results in the conservation of energy $2E_P = E_S + E_I$, and momenta $2\mathbf{k}_P = \mathbf{k}_S + \mathbf{k}_I$ where \mathbf{k} is the wavevector. The scattering is resonant to the eigenstates of the system, which in the investigated sample are the polaritons of the lower, middle and upper branches with the energies $E_{LP}(\mathbf{k})$, $E_{MP}(\mathbf{k})$, $E_{UP}(\mathbf{k})$. This scattering enables optical parametric amplification³. A theoretical model describing the spontaneous parametric fluorescence was discussed in Ref. 4, and extended to stimulated emission in Ref. 5. Spontaneous parametric emission was experimentally investigated in Ref. 6,7 showing the scattering into the phase-matched 8-shapes in momentum space, which was then shown to provide entangled photon sources^{7,8}, which was recently extended to one-dimensional cavity structures^{9,10}. In this letter, we report on spontaneous parametric scattering of resonantly excited polaritons onto real and ghost branches.

The microcavity sample¹¹ investigated here is a 1λ $\text{Al}_{0.05}\text{Ga}_{0.95}\text{As}$ cavity with a single 15 nm GaAs quantum well with 5 nm $\text{Al}_{0.3}\text{Ga}_{0.7}\text{As}$ barriers in its center, providing two excitonic resonances, the heavy hole and the light hole exciton. The cavity is surrounded by $\text{AlAs}/\text{Al}_{0.15}\text{Ga}_{0.85}\text{As}$ distributed Bragg reflectors with 25(16) periods on the bottom(top) of the epilayer. The cavity mode energy gradient was about 1.5 meV/mm, which allowed to adjust the detuning between cavity and heavy-hole exciton $\Delta_c = E_c - E_{hh}$. The use of a wide binary GaAs well eliminates the alloy disorder found in In-GaAs/GaAs quantum wells¹², resulting in an inhomogeneous exciton linewidth of¹¹ 170 μeV . The $\text{Al}_{0.05}\text{Ga}_{0.95}\text{As}$ cavity reduces the carrier confinement and thus the carrier trapping and the related homogenous broadening¹³. The resulting exciton linewidth was measured here at full-width half maximum as $\gamma_{hh} = 150 \mu\text{eV}$ using re-

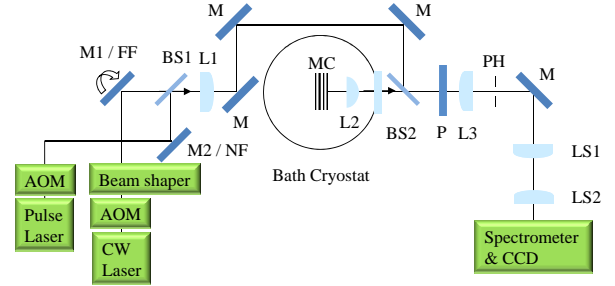


FIG. 1: Optical setup used. M1,M2: Gimbal mounted mirrors, L1-L6 Lenses, MC: Microcavity sample, LS1,LS2 movable lenses for imaging, dashed lines: removable mirrors, BS1,BS2 Beam-splitters.

flection spectroscopy. The cavity linewidth γ_c of about 300 μeV is limited by the reflectivity of the top Bragg mirror.

The sample was mounted in a helium bath cryostat at a temperature of 5 K and a vapor pressure of 200 mbar. To measure the polariton dispersion, we used a weak pulsed excitation with a mode-locked Ti:Sapphire laser (Coherent Mira) delivering 100 fs pulses at 76 MHz repetition rate and a spectral width of approximately 20 meV. The excitation was focused to a diffraction limited spot of 1.5 μm with a 0.5NA lens having a wavevector range of $|k| \leq 4/\mu\text{m}$. To excite pump polaritons for parametric scattering, we used a linearly polarized single-mode CW external cavity diode laser with a spectral width of 20 neV. Two-dimensional excitation wavevector control was realized by a mirror on a gimbal mount, which was imaged onto the sample⁶. The beam divergence at the mirror was adjusted to create a gaussian tail at the sample, providing the minimum wavevector spread for a given excitation size. The beam diameter at $1/e$ intensity on the sample was 70 μm , corresponding to a wavevector spread of $|k| \leq 0.09/\mu\text{m}$. In order to avoid sample heating, the excitation was chopped by an acousto-optic modulator producing pulses of 1 μs pulse duration at 1% duty cycle. The peak intensity on the sample I was about 10^3 W/cm^2 . The resonantly created polariton density $N_{LP}(\mathbf{k}_P) \simeq I\tau T/E_P \simeq 10^7/\text{cm}^2$ ²⁰ The reciprocal space (\mathbf{k}) of the cross-linearly polarized emission was imaged onto the input slit of a high resolution (20 μeV) imaging spectrometer and detected using a CCD-Camera^{14,15}.

The polariton dispersion in the low-intensity regime

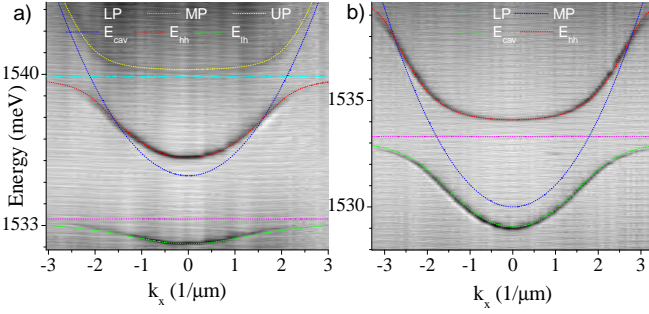


FIG. 2: Reflection of the microcavity as function of photon energy and wavevector $\mathbf{k} = (k_x, 0)$. a) positive detuning $\Delta_c = 5$ meV. b) negative detuning $\Delta_c = -4$ meV. The calculated polariton dispersions $\tilde{E}_B(\mathbf{k})$ are given by lines as labeled.

was measured using \mathbf{k} resolved reflection spectroscopy as shown in Fig. 2, and modeled with the coupled three oscillator model for the cavity mode, heavy- and light-hole exciton^{13,16}. From these fits of $E_B(\mathbf{k})$ to the set of polariton branches $B = \{LP, MP, UP\}$, we deduced the exciton energies $E_{hh} = 1.5333$ eV, $E_{lh} = 1.5399$ eV, and the Rabi splittings $2\Omega_{hh} = 3.7$ meV, $2\Omega_{lh} = 2.4$ meV, for heavy- and light-hole excitons, respectively. The exciton and polariton linewidths of this sample were previously compared¹¹ with the linewidth averaging model, in which the polariton linewidth γ_B is a weighted average of γ_c and the exciton linewidths γ_{hh}, γ_{lh} ,

$$\gamma_B = x_{lh,B}\gamma_{hh} + x_{hh,B}\gamma_{lh} + c_B\gamma_c \quad (1)$$

with the contents of cavity c_B , heavy hole exciton $x_{hh,B}$, and light hole exciton $x_{lh,B}$ in the polariton¹⁷. The model is assuming Lorentzian lineshapes, and shows sufficient agreement¹¹ with the experiment for the LP at zero and negative detuning. Increasing the exciton density as relevant in our experiments, the exciton linewidth is dominated by exciton-exciton scattering, which has a different non-Lorentzian shape compared to inhomogeneous broadening.

The parametric emission was modeled following Ref. 4, where the polaritons are excited resonantly with a pump field $P_P(t) = \langle p_{LP}^\dagger(\mathbf{k}_P, t) \rangle$ of defined wavevector \mathbf{k}_P and photon energy E_P within the LP branch. The polaritons of signal and idler are coupled by a momentum conserving exciton-exciton scattering proportional to the pump intensity, described by off-diagonal terms in an anti-hermitian coupling matrix. In the following we use the renormalised complex polariton energies $\tilde{E}_B = E_B - i\gamma_B + E_B^{\text{ren}}|P_P|^2$. The polariton-polariton interaction term E_B^{ren} was determined using Eq. 9 in Ref. 6

$$E_B^{\text{ren}}(\mathbf{k}) = 2x_{LP}(\mathbf{k}_P)x_B(\mathbf{k}) \left\{ 12E_X + \frac{16\pi}{7}\Omega_{hh} \left[\sqrt{x_{LP}^{-1}(\mathbf{k}_P) - 1} + \sqrt{x_B^{-1}(\mathbf{k}) - 1} \right] \right\}, \quad (2)$$

with an exciton binding energy of $E_X = 8$ meV. The excitonic content x_B was taken as the sum $x_B = x_{hh,B} + x_{lh,B}$ of heavy and light hole content. The expression holds for circular polarization, so that for the cross-linear polarization configuration used here in the regime where the

renormalisation is smaller than the linewidth we expect some deviations in the overall scattering strength. For higher polariton densities the spin-dependent interaction is influencing the dynamics significantly¹⁸

Neglecting higher-order scattering processes and Langevin terms of the external light field, the steady-state emission from these branches was derived in an analytical form (Eq. 9 of Ref. 4) as a function of the steady state population of the signal $N_B(\mathbf{k}_S) = \langle p_B^\dagger(\mathbf{k}_S, 0)p_B(\mathbf{k}_S, 0) \rangle$ and an anomalous parametric correlation amplitude between signal and idler polaritons $A_B^*(\mathbf{k}_S) = \langle p_B^\dagger(\mathbf{k}_S, 0)p_B^\dagger(\mathbf{k}_I, 0) \rangle$ where $p_B(\mathbf{k}, t)$ is the time-dependent polariton operator of branch B and wavevector \mathbf{k} . We extended the model to include the middle polariton branch (MP) resulting in a corresponding ghost branch (MP*). The coupling matrix for the different branches is given by

$$M_B^{\text{par}} = \begin{pmatrix} \hat{E}_B(\mathbf{k}_S) & E_B^{\text{int}}P_P^2 \\ -(E_B^{\text{int}}P_P^2)^* & 2E_P - \hat{E}_B^*(\mathbf{k}_I) \end{pmatrix} \quad (3)$$

having the eigenvalues $\hat{E}_B^\pm(\mathbf{k}_S)$. The interaction energy E_B^{int} is given by Eq. 8 in Ref. 6,

$$E_B^{\text{int}}(\mathbf{k}_S) = x_{LP}(\mathbf{k}_P)\sqrt{x_B(\mathbf{k}_S)x_B(\mathbf{k}_I)} \times \left\{ 12E_X + \frac{16\pi}{7}\Omega_{hh} \left[2\sqrt{x_{LP}^{-1}(\mathbf{k}_P) - 1} + \sqrt{x_B^{-1}(\mathbf{k}_S) - 1} + \sqrt{x_B^{-1}(\mathbf{k}_I) - 1} \right] \right\}, \quad (4)$$

The parametric emission intensity of each polariton branch I_B^{par} is then given by

$$I_B^{\text{par}}(\mathbf{k}_S, \omega) \propto c_B(\mathbf{k}_S) \times \Im \left\{ \frac{\Delta_B(\mathbf{k}_S, \omega)N_B(\mathbf{k}_S) + E_B^{\text{int}}(\mathbf{k}_S)P_P^2A_B^*(\mathbf{k}_S)}{(\hat{E}_B^+(\mathbf{k}_S) - \hbar\omega)(\hbar\omega - \hat{E}_B^-(\mathbf{k}_S))} \right\} \quad (5)$$

with

$$A_B^*(\mathbf{k}_S) = \frac{E_B^{\text{int}}(\mathbf{k}_S)P_P^2\delta_B(\mathbf{k}_S)}{|\delta_B(\mathbf{k}_S)|^2 - \frac{(\gamma_B(\mathbf{k}_S) + \gamma_B(\mathbf{k}_I))^2}{\gamma_B(\mathbf{k}_S)\gamma_B(\mathbf{k}_I)} |E_B^{\text{int}}(\mathbf{k}_S)P_P^2|^2},$$

$N_B(\mathbf{k}_S) = \Im \{ E_B^{\text{int}}(\mathbf{k}_S)P_P^2A_B^*(\mathbf{k}_S) \} / \gamma_B(\mathbf{k}_S)$, the emission detuning $\Delta_B(\mathbf{k}_S, \omega) = \hbar\omega + \hat{E}_B^*(\mathbf{k}_I) - 2E_P$ and the signal-idler detuning $\delta_B(\mathbf{k}_S) = 2E_P - \hat{E}_B^*(\mathbf{k}_S) - \hat{E}_B^*(\mathbf{k}_I)$. The total emission I^{par} is the sum of I_B^{par} over all branches B. This theoretical treatment is valid below the threshold for parametric oscillation given by the condition $\Im(\hat{E}_B^-(\mathbf{k}_S)) < 0$. We used the complex polariton energies \tilde{E}_B calculated in the three coupled oscillator model with a k-dependent broadening from Eq.(1) with $\gamma_c = 300\mu\text{eV}$ and $\gamma_{lh} = \gamma_{hh} = 400\mu\text{eV}$. The exciton linewidths are higher than measured in the low intensity regime, which we attribute to exciton-exciton scattering by the higher exciton density in the parametric scattering experiments¹⁹. The pump is assumed to be resonant to the LP branch. The simulations shown are well below the

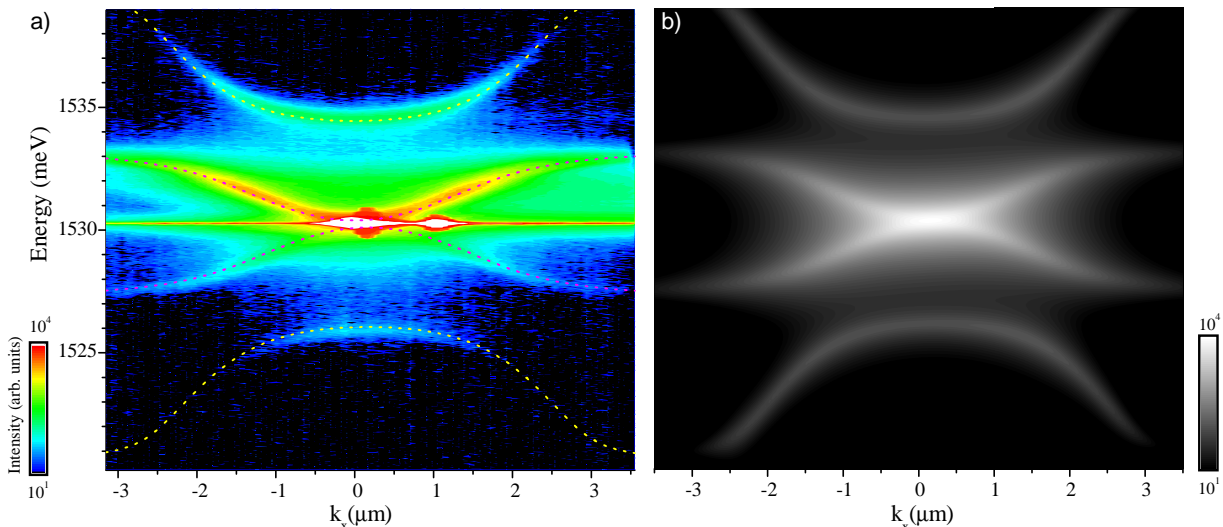


FIG. 3: Energy and wavevector resolved emission intensity $I(\mathbf{k}, \omega)$ on a logarithmic scale as indicated, for a pump energy $E_P = 1530.25$ meV and wavevector $\mathbf{k}_P = (0.1, 0)/\mu\text{m}$ at a cavity detuning of $\Delta_c = -1.7$ meV. a) Measured $I(\mathbf{k}, \omega)$ for $\mathbf{k} = (k_x, 0.4/\mu\text{m})$. Lines: Eigenmodes $\hat{E}_B^\pm(\mathbf{k})$ of Eq.(3), for B=LP in magenta, and for B=MP in yellow. b) Parametric emission $I^{\text{par}}(\mathbf{k}, \omega)$ calculated using Eq.(5).

threshold, for which the renormalization is negligible and I^{par} is independent of the pump intensity up to a scaling factor. We used $P_{\mathbf{k}_P} = 10^{-3}$, $N_{LP}(\mathbf{k}_P) \simeq 10^8/\text{cm}^2$ for exciton Bohr radius $\lambda_X = 14$ nm⁴. Simulations were made with a step size of $20 \mu\text{eV}$ in $\hbar\omega$ and $0.06/\mu\text{m}$ in \mathbf{k}_s .

We now discuss the measured microcavity emission for different pump energies and wavevectors together with corresponding results of simulations. We commence with a pump close to the dispersion minimum at $E_P = 1530.15$ meV and $\mathbf{k}_P = (0.1, 0)/\mu\text{m}$ for a cavity detuning $\Delta_c = -1.7$ meV, shown in Fig. 3. The measured emission $I((k_x, 0.4/\mu\text{m}), \omega)$ shown in Fig. 3a shows the dominant emission from the LP and from the pump which is scattered elastically by disorder towards the detection wavevector range. The emission from the MP is about 2 orders of magnitude weaker, and the ghost branches LP* and MP* are 2-4 orders of magnitude weaker and show a reversed dispersion. The corresponding predicted eigenvalues $\hat{E}_B^\pm(\mathbf{k})$ of Eq.(3) are following the observed emission peaks. For a more detailed comparison with theory, we give in Fig. 3b the calculated parametric emission intensity I^{par} , which shows a semi-quantitative agreement with the experimental result. The main deviation is the observed intensity of the ghost branches, which in the experiment is much weaker than in the simulation. This is actually expected as the model accounts for radiative broadening only, such that all parametrically scattered polaritons are emitted, resulting in equal intensities of signal and idler. In the experiment, a significant part of the broadening at higher \mathbf{k} is due to the exciton linewidth (see Eq.(1)), which represents a scattering of polaritons into excitonic states. This scattering results in a thermalized population of excitons at high \mathbf{k} , emitting dominantly from the LP and the bottleneck region, which is the reason for the observed strong LP emission. Ghost branches are best visible for small \mathbf{k}_P due to the smaller

contribution of the exciton broadening¹⁹.

Moving the pump away from the dispersion minimum to $\mathbf{k}_P = (0.85, 0)/\mu\text{m}$, the emission reveals the expected asymmetry as shown in Fig. 4. Two different cross-sections $\mathbf{k} = (k_x, 0.3/\mu\text{m})$ in (a,b) and $\mathbf{k} = (0/\mu\text{m}, k_y)$ in (c,d) of the full three-dimensional data set are given. Moving further along the dispersion to $\mathbf{k}_P = (0, -1.9)/\mu\text{m}$ close to the inflexion point, as shown in Fig. 5, LP and LP* intersect close to the dispersion minimum at $\mathbf{k}_P = (0, -0.5)/\mu\text{m}$ and $\mathbf{k}_P = (0, 0.2)/\mu\text{m}$, at which energy and momentum conserving scattering is resonant for signal and idler. This pump wavevector is close to the so-called magic angle³ for which LP and LP* intersect at $\mathbf{k} = 0$ resulting in a small threshold for parametric oscillation. For this excitation the ghost branches are visible mainly at the intersection points. This could partly be due to the onset of stimulated scattering¹⁷. The corresponding simulations shown in Fig. 5b give good agreement with measurement for the LP branch. However, the calculated MP branch has a weaker emission for small \mathbf{k} , and a higher emission for large \mathbf{k} . This is again related to the exciton scattering into the exciton reservoir and subsequent emission of thermalized excitons, as the middle polariton the highest exciton content at small \mathbf{k} .

In Fig. 6, we show measured polariton luminescence for $\mathbf{k}_P = (0, -1.95)/\mu\text{m}$ well above the inflexion point, resulting in an 8-shaped resonant region⁶ in \mathbf{k} space. In the cross-section $\mathbf{k} = (-0.25/\mu\text{m}, k_y)$, the LP real and ghost branches intersect at $E = 1526.95$ meV, $\mathbf{k} = (-0.25, 0.7)/\mu\text{m}$. In the cross-section $\mathbf{k} = (k_x, 0)$ shown in Fig. 6c, the LP real and ghost branches intersect at $E = 1527.1$ meV, $\mathbf{k} = (\pm 0.82, 0)/\mu\text{m}$. Again a good agreement with the simulations is found.

In summary we have shown polariton parametric pair scattering from a resonantly excited pump state into real and ghost branches of signal and idler polaritons for dif-

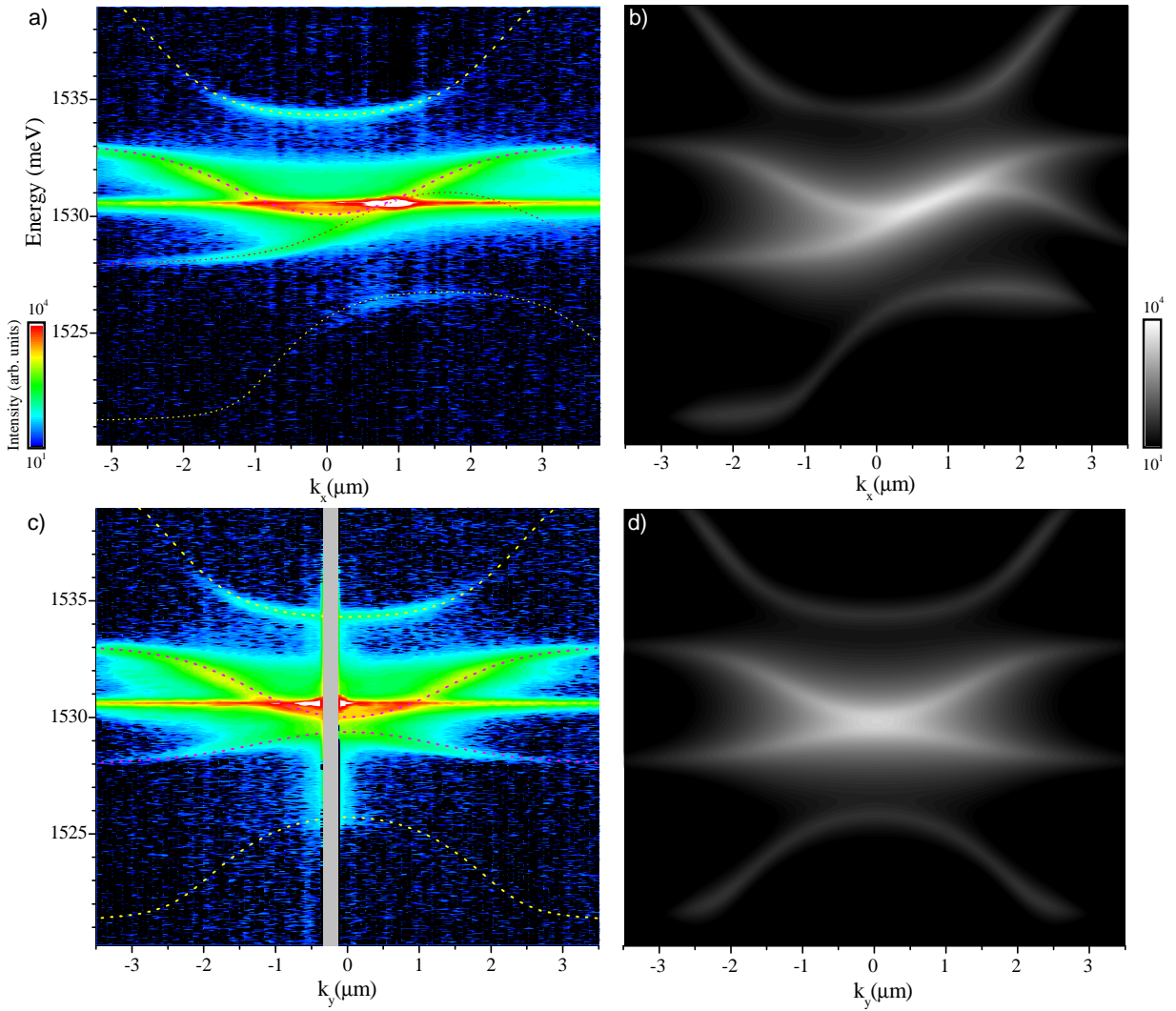


FIG. 4: As Fig. 3, but for $E_P = 1530.55$ meV, $\mathbf{k}_P = (0.85, 0)/\mu\text{m}$, $\Delta_c = -2.1$ meV. a,b) $\mathbf{k} = (k_x, 0.3/\mu\text{m})$. c,d) $\mathbf{k} = (0/\mu\text{m}, k_y)$.

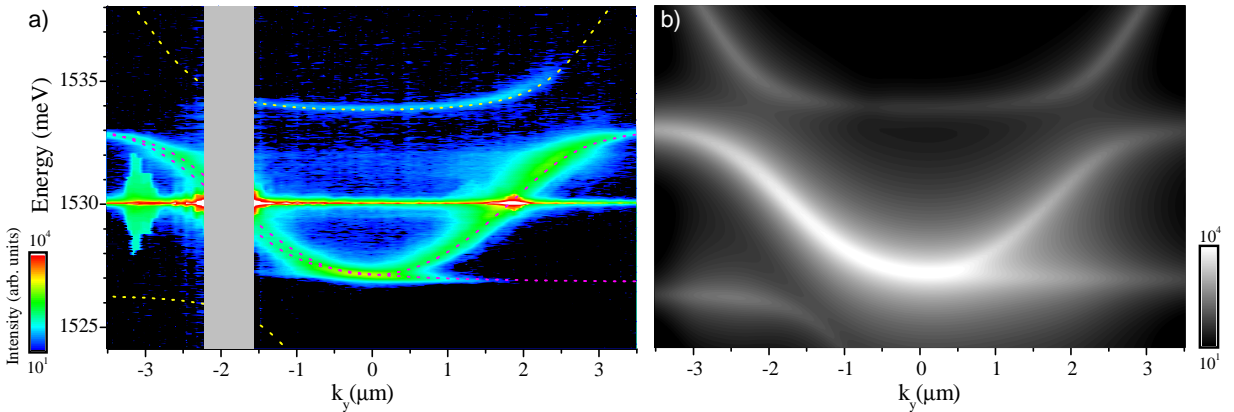


FIG. 5: As Fig. 3, but for $E_P = 1530.1$ meV, $\mathbf{k}_P = (0, -1.9)/\mu\text{m}$, $\Delta_c = -5.5$ meV, and cross-section $\mathbf{k} = (0, k_y)$.

ferent excitation angles and wavevectors. The measurements are in agreement with simulations, apart from the additional emission due to thermalized excitons and the missing treatment of non-radiative decay. These results can be further explored towards entangled photon source by measurements of their time-correlation.

Acknowledgments

This work was supported by the EPSRC under grant n. EP/F027958/1.

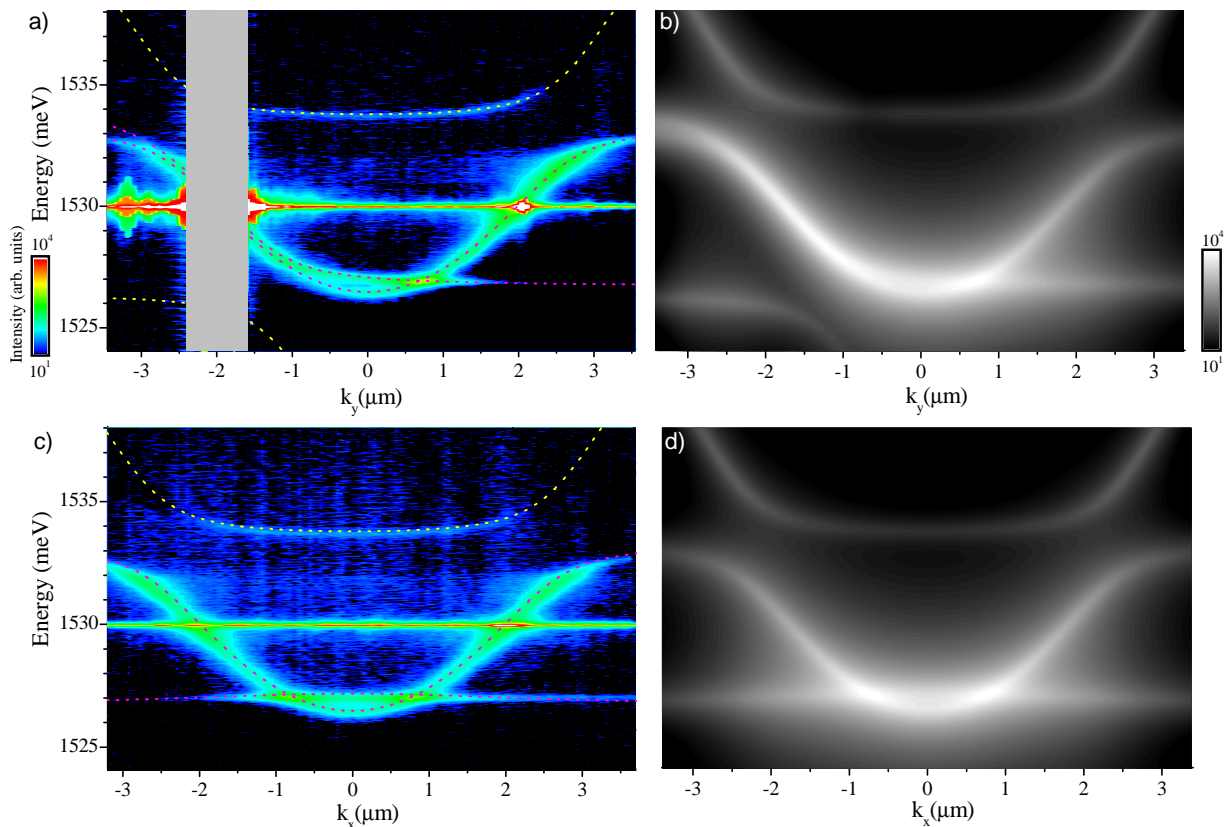


FIG. 6: As Fig. 3 but for $E_P = 1530.0$ meV, $\mathbf{k}_P = (0, -1.95)/\mu\text{m}$, $\Delta_c = -6$ meV, and $\mathbf{k} = (-0.25/\mu\text{m}, k_y)$ for a,b and $\mathbf{k} = (k_x, 0)$ in (c,d), $\delta k = 0.14/\mu\text{m}$.

-
- * Electronic address: joanna.m.zajac@gmail.com
- ¹ A. Kavokin, J. Baumberg, G. Malpuech, and F. Laussy, *Microcavities*, Series on Semiconductor Science and Technology (OUP Oxford, 2007), ISBN 9780191620737.
 - ² R. W. Boyd, *Nonlinear Optics* (Academic Press, 2008).
 - ³ P. G. Savvidis, J. J. Baumberg, R. M. Stevenson, M. S. Skolnick, D. M. Whittaker, and J. S. Roberts, *Phys. Rev. Lett.* **84**, 1547 (2000).
 - ⁴ C. Ciuti, P. Schwendimann, and A. Quattropani, *Phys. Rev. B* **63**, 4, 5 (2001), parametric.
 - ⁵ C. Ciuti, P. Schwendimann, and A. Quattropani, *Semicond. Sci. Technol.* **18**, S279 (2003).
 - ⁶ W. Langbein, *Phys. Rev. B* **70**, 205301 (2004).
 - ⁷ W. Langbein, *Phys. Status Solidi B* **242**, 2260 (2005).
 - ⁸ S. Savasta, O. D. Stefano, V. Savona, and W. Langbein, *Phys. Rev. Lett.* **94**, 246401 (2005).
 - ⁹ M. Abbarchi, V. Ardizzone, T. Lecomte, A. Lemaitre, I. Sagnes, P. Senellart, J. Bloch, P. Roussignol, and J. Tignon, *Phys. Rev. B* **83**, 201310 (2011).
 - ¹⁰ V. Ardizzone, M. Abbarchi, T. Lecomte, A. Lemaitre, I. Sagnes, P. Senellart, J. Bloch, P. Roussignol, and J. Tignon, *Phys. Status Solidi B* **249**, 896 (2012).
 - ¹¹ P. Borri, W. Langbein, U. Woggon, J. R. Jensen, and J. M. Hvam, *Phys. Rev. B* **63**, 035307 (2001).
 - ¹² J. R. Jensen, J. M. Hvam, and W. Langbein, *J. Appl. Phys.* **86**, 2584 (1999).
 - ¹³ J. R. Jensen, P. Borri, W. Langbein, and J. M. Hvam, *Appl. Phys. Lett.* **76**, 3262 (2000).
 - ¹⁴ J. M. Zajac, W. Langbein, M. Hugues, and M. Hopkinson, *Phys. Rev. B* **85**, 165309 (2012).
 - ¹⁵ W. Langbein, *Rivista del nuovo cimento* **33**, 255 (2010).
 - ¹⁶ W. Langbein, *J. Phys.: Condens. Matter* **16**, S3645 (2004).
 - ¹⁷ W. Langbein, P. Borri, U. Woggon, V. Stavarache, D. Reuter, and A. D. Wieck, *Phys. Rev. B* **70**, 033301 (2004).
 - ¹⁸ D. D. Solnyshkov, I. A. Shelykh, N. A. Gippius, A. V. Kavokin, and G. Malpuech, *Phys. Rev. B* **77**, 045314 (2008).
 - ¹⁹ A. Huynh, J. Tignon, O. Larsson, P. Roussignol, C. Delalande, R. André, R. Romestain, and L. S. Dang, *Phys. Rev. Lett.* **90**, 106401 (2003).
 - ²⁰ N_{LP} was calculated using the lower polariton lifetime $\tau = \hbar/\gamma_{LP} = 1.5$ ps with $\gamma_{LP} = 400$ μeV , and the DBR top mirror transmission for $\gamma_{cav} = 300$ μeV was calculated as $T = 0.3\%$